Tracking of High-speed, Non-smooth and Microscale-amplitude Wave Trajectories

Jiradech Kongthon
Department of Mechatronics Engineering, Assumption University, Suvarnabhumi Campus, Samuthprakarn, Thailand

Keywords: High-speed Tracking, Inversion-based Control, Microscale Positioning, Reduced-order Inverse, Tracking.

Abstract: In this article, an inversion-based control approach is proposed and presented for tracking desired trajectories with high-speed (100Hz), non-smooth (triangle and sawtooth waves), and microscale-amplitude (10 micron) wave forms. The interesting challenge is that the tracking involves the trajectories that possess a high frequency, a microscale amplitude, sharp turnarounds at the corners. Two different types of wave trajectories, which are triangle and sawtooth waves, are investigated. The model, or the transfer function of a piezoactuator is obtained experimentally from the frequency response by using a dynamic signal analyzer. Under the inversion-based control scheme and the model obtained, the tracking is simulated in MATLAB. The main contributions of this work are to show that (1) the model and the controller achieve a good tracking performance measured by the root mean square error (*RMSE*) and the maximum error (E_{max}), (2) the maximum error occurs at the sharp corner of the trajectories, (3) tracking the sawtooth wave yields larger *RMSE* and E_{max} values,compared to tracking the triangle wave, and (4) in terms of robustness to modeling error or unmodeled dynamics, E_{max} is still less than 10% of the peak to peak amplitude of 20 micron if the increases in the natural frequency and the damping ratio are less than 5% for the triangle trajectory and E_{max} is still less than 10% of the peak to peak amplitude of 20 micron if the increases in the natural frequency and the damping ratio are less than 3.2 % for the sawtooth trajectory.

1 INTRODUCTION

A piezo stage is widely used in positioning and actuating motions in nano/microscale displacements or amplitudes. Several works have used a piezoactuator to achieve the goals. For example, the works done by Kongthon et al., (2010, 2011 and 2013) employed a piezo-based positioning system to drive the biomimetic cilia-based device so that the mixing performance in a micro device was improved. Moallem et al., (2004) used piezoelectric devices for the flexure control of a positioning system.

The tracking of a trajectory is very common in control problems such as the works by Beschi et al., (2014) and Martin et al., (1996). Tracking can be challenging in high-frequency applications with very small displacements. The challenge in this work is that the trajectories are of high-speed (100Hz), non-smooth (triangle and sawtooth waves), and microscale-amplitude (10 micron) wave forms. The goal is to propose a controller that can track prescribed trajectories properly with a good tracking performance. The tracking performance can be measured by the root mean square error (*RMSE*) and the maximum error (E_{max}).

The rest of this article is structured as follows. Section 2 introduces the two trajectories. The piezoactuator model is obtained in section 3. The control scheme is proposed in section 4. Section 5 shows the results. In section 6, the robustness is investigated. Section 7 concludes the article.

2 TRAJECTORIES

2.1 The Trajectories to Be Tracked

In this work, there are two types of wave form trajectories used to investigate the tracking performance of the piezoactuator model: triangle wave, shown in Fig. 1 and sawtooth wave, shown in Fig. 2.

Kongthon, J.
Tracking of High-speed, Non-smooth and Microscale-amplitude Wave Trajectories.
DOI: 10.5220/0005979704990507
In *Proceedings of the 13th International Conference on Informatics in Control, Automation and Robotics (ICINCO 2016) - Volume 1*, pages 499-507
ISBN: 978-989-758-198-4

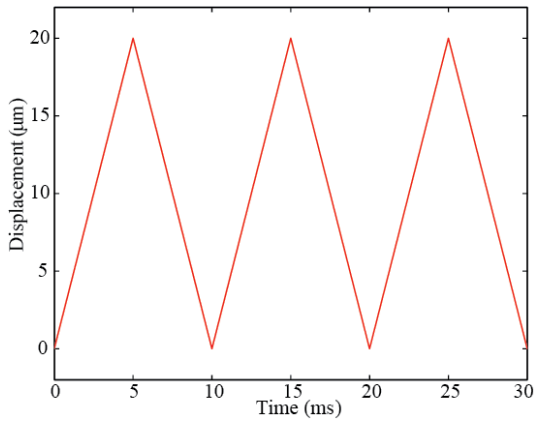

Figure 1: Original trajectory for triangle wave of 10 μm amplitude and 100 Hz frequency

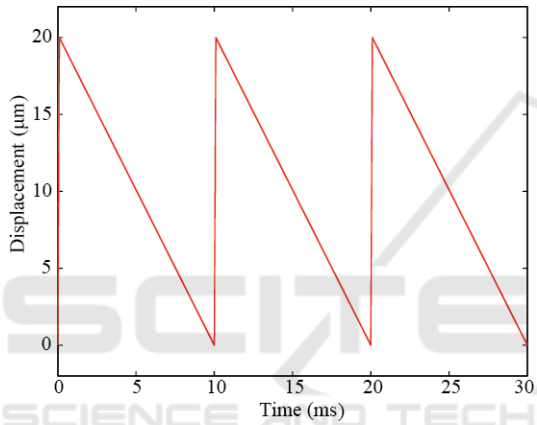

Figure 2: Original trajectory for sawtooth wave of 10 μm amplitude and 100 Hz frequency

2.2 Filtered and Desired Trajectories

It can be seen in Figs. 1 and 2 that the original trajectories contain very sharp turnarounds at the corners. In practice, an actuator cannot track a trajectory with a very sharp corner properly as it has a limited bandwidth. In order to achieve a good tracking performance, the original trajectories therefore need to be smoothen by a second-order filter with the filtering transfer function of the form.

$$G_f(s) = \left(\frac{\omega_f}{s+\omega_f}\right)\left(\frac{\omega_f}{s+\omega_f}\right)$$

where ω_f is the break frequency of the filter , and In this work, ω_f of 10 Hz, or $10(2\pi)$ rad/s is selected to get the trajectories filtered. The filtered trajectory is hereafter referred to as the desired trajectory. The controller then needs to track the desired trajectory of each type.

3 PIEZO ACTUATOR MODEL

A piezo-based positioning system, or piezo stage, can be used in applications that require very small displacements and large frequency ranges. A piezoactuator can generate an extremely small displacement down to the subnanometer range.

The number of vibration modes for the piezo stage is infinite since the beam mechanism inside the piezo stage has an infinite dimension. In general, an infinite dimensional plant can be approximated by a finite dimensional model, and in practice, it is possible to take the first few modes of vibration to represent the total dynamics of the plant.

3.1 Frequency Response Experiment

To obtain the model of the piezoactuator shown in Fig. 3, the piezoactuator and the dynamic signal analyzer shown in Fig. 4, together with an inductive sensor and a power amplifier are connected as shown in Fig. 5 to get the frequency response, and the model is then obtained.

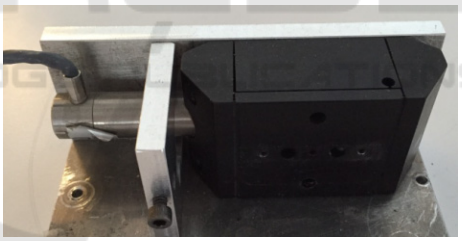

Figure 3: Piezoactuator used to produce micro-scale amplitudes of oscillations with high frequencies.

Figure 4: Dynamic signal analyzer used to get the frequency response to obtain the model of the actuator.

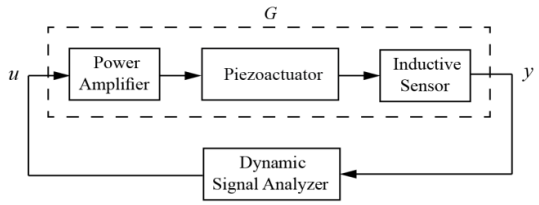

Figure 5: Block diagram used for obtaining the frequency response of the piezoactuator.

3.2 Transfer Function and Time Scaling

In this work, the poles, the zeros, and the gain of the piezoactuator are found experimentally and the experimental result from the frequency response shows that the model is composed of 6 poles and 4 zeros in the frequency range of 0 to 1000 Hz.

The poles are located in the complex s-plane at

$$\begin{bmatrix} p_1, p_2 \\ p_3, p_4 \\ p_5, p_6 \end{bmatrix} = \begin{bmatrix} -346.8 \pm 1952.7\mathrm{i} \\ -169.4 \pm 4149.2\mathrm{i} \\ -65.9 \pm 5361.0\mathrm{i} \end{bmatrix} \quad (1)$$

The zeros are located in the complex s-plane at

$$\begin{bmatrix} z_1, z_2 \\ z_3, z_4 \end{bmatrix} = \begin{bmatrix} -159.6 \pm 4027.3\mathrm{i} \\ -49.7 \pm 5397.6\mathrm{i} \end{bmatrix} \quad (2)$$

The constant gain is

$$K = 1.1879\mathrm{x}\ 10^7 \quad (3)$$

The poles and the zeros specify and define the properties of the transfer function, thus describing the input-output system dynamics. The poles, the zeros, and the gain K all together completely provide a full description of the system and characterize the system dynamics and the response.

The transfer function can now be constructed by using the poles, the zeros, as well as the gain, and the resulting transfer function $G(s)$ is found to be of the form.

$$G(s) = \frac{1.188(10^7)s^4 + 4.973(10^9)s^3 + 5.395(10^{14})s^2 + \cdots}{s^6 + 1.164(10^3)s^5 + 5.03(10^7)s^4 + 4.58(10^{10})s^3 \cdots} \frac{1.297(10^{17})s + 5.622(10^{21})}{6.851(10^{14})s^2 + 3.911(10^{17})s + 1.95(10^{21})} \quad (4)$$

The DC gain of the system in dB is equal to $20log_{10}(5.622\mathrm{x}10^{21}/1.95\mathrm{x}10^{21}) = 9.20$ dB.

The inspection of Eq.(4) indicates that the system response is very fast with the settling time in milliseconds. To avoid numerical problems with simulations in MATLAB, the time unit needs to be changed from second to millisecond. To do this, each variable, s, in the transfer function in Eq.(4) is replaced by 1000s ,and the new transfer function $G_{ms}(s)$ in terms of millisecond is obtained as

$$G_{ms}(s) = \frac{11.88s^4 + 4.973s^3 + 539.5s^2 + \cdots}{s^6 + 1.164s^5 + 50.3s^4 + 45.8s^3 \cdots} \frac{129.7s + 5622}{685.1s^2 + 391.1s + 1950} \quad (5)$$

The s variable in the new transfer function in Eq.(5) has the unit in radian/millisecond. In MATLAB, the time axis must therefore be rescaled to millisecond. The Bode diagram that represents the frequency response of the piezoactuator is plotted by using $G_{ms}(s)$ and illustrated in Fig. 6.

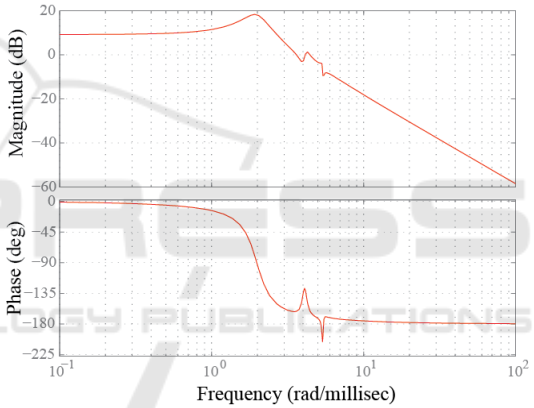

Figure 6: Bode diagram of the piezoactuator.

In this work, the sixth-order model of the actuator is decomposed into three modes of second-order systems by using the parallel state space realization method, shown in Fig.7 so that robustness can be investigated by providing each mode with variations in the natural frequency and the damping ratio.

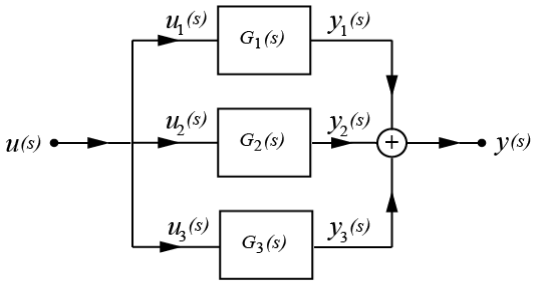

Figure 7: Diagram for parallel state space realization, an approach to decoupling the modes of oscillations.

To find the state space representation by the parallel state space realization method, the transfer function can be rewritten in the form of partial fractions.

$$\frac{y(s)}{u(s)} = \frac{r_1}{s-p_1} + \frac{r_2}{s-p_2} + \frac{r_3}{s-p_3} + \frac{r_4}{s-p_4} + \ldots + \frac{r_5}{s-p_5} + \frac{r_6}{s-p_6} + k_s \quad (6)$$

where r_1, $r_2, \ldots r_6$ are the residues, p_1, $p_2, \ldots p_6$ are the poles of the system, and k_s is the direct term.

The direct term is equal to zero for a strictly proper transfer function. The poles located at $s = p_1$, p_2, …, p_6 are shown in Eq.(1), and it follows that

$$G_{ms}(s) = \frac{y(s)}{u(s)} = G_{ms,1}(s) + G_{ms,2}(s) + G_{ms,3}(s) \quad (7)$$

Where $G_{ms,1}(s)$, $G_{ms,2}(s)$, and $G_{ms,3}(s)$ are obtained as follows.

$$G_{ms,1}(s) = \frac{-0.0511s + 11.1660}{s^2 + 0.6938s + 3.9344} \quad \text{for mode 1}$$

$$G_{ms,2}(s) = \frac{0.0397s + 0.8986}{s^2 + 0.3388s + 17.2312} \quad \text{for mode 2}$$

$$G_{ms,3}(s) = \frac{0.0114s - 0.2050}{s^2 + 0.1315s + 28.7637} \quad \text{for mode 3}$$

Now, the system is decoupled to three modes, and each mode is represented by a second-order transfer function. The system in Eq.(7) represents the original system described by Eq.(5) and preserves the original system response characteristics.

A second-order system possesses a pair of complex conjugate poles and the pole location determines the natural frequency and the damping ratio. For a second-order system, the location of the poles s_1, s_2 is related to the natural frequency ω_n and the damping ratio ζ by

$$s_1, s_2 = -\zeta\omega_n \pm i\omega_n\sqrt{1-\zeta^2} \quad (8)$$

From the pole locations and Eq.(8) above, the natural frequency ω_n and the damping ratio ζ for each mode of vibration can be found and shown in Table 1. It is noted that the system is stable since all the poles have a negative real part, and the mode number is determined by realizing that the higher mode number will have a greater natural frequency.

Table 1: Pole location, natural frequency and damping ratio for each mode.

Pole Location	ω_n (Hz)	ζ	Mode
p_1 = -346.8 + 1952.7i	315.65	0.175	1
p_2 = -346.8 – 1952.7i	315.65	0.175	1
p_3 = -169.4 + 4149.2i	660.92	0.041	2
p_4 = -169.4 – 4149.2i	660.92	0.041	2
p_5 = -65.9 + 5361.0i	853.29	0.012	3
p_6 = -65.9 – 5361.0i	853.29	0.012	3

4 CONTROL SCHEME

The notions and the developments of inversion-based control have attracted researchers in the field and have been around for more than four decades. The early and remarkable works on inversion-based approach were presented by Silverman (1969) and Hirschorn (1979). Later on, many developments and contributions were made by means of inversion-based control, or feedforward control methods such as the works by Peng et al., (1993), Meckl et al., (1994), Piazzi et al., (2001), Devasia (2002), Dunne et al., (2011), Yang et al., (2011) and Boekfah et al., (2016). The standard inversion control theory is based on a known or pre-described trajectory.

In this work, the trajectories are prescribed or known a priori and the system is a minimum phase type and is stable. The inversion-based control approach is hence suited and proposed for tracking the desired trajectories.

4.1 State Space Representation

It is well known that for a linear time-invariant system (LTI system), the plant dynamics can be represented by the state equation of the form.

$$\dot{x}(t) = Ax(t) + Bu(t) \quad (9)$$

and the output equation of the form.

$$y(t) = Cx(t) + Du(t) \quad (10)$$

For a strictly proper system such as the case here, D is equal to zero.

Now $G_{ms,1}(s)$, $G_{ms,2}(s)$, and $G_{ms,3}(s)$ in Eq.(7) can be cast into the state space form of Eq. (9) and Eq. (10), and matrices A, B, C, and D are as follows.

$$A=\begin{bmatrix} 0 & 1 & 0 & 0 & 0 & 0 \\ -3.9344 & -0.6938 & 0 & 0 & 0 & 0 \\ 0 & 0 & 0 & 1 & 0 & 0 \\ 0 & 0 & -17.2312 & -0.3388 & 0 & 0 \\ 0 & 0 & 0 & 0 & 0 & 1 \\ 0 & 0 & 0 & 0 & -28.7637 & -0.1315 \end{bmatrix}$$

$$B=\begin{bmatrix} 0 \\ 1 \\ 0 \\ 1 \\ 0 \\ 1 \end{bmatrix}$$

$$C=\begin{bmatrix} 11.166 & -0.0511 & 0.8986 & 0.0397 & -0.2050 & 0.0114 \end{bmatrix}$$

$$D=0$$

4.2 Inversion-based Control Approach

The relative degree, *r,* of the system is defined by the difference between the number of poles and the number of zeros. For the model governed by Eq.(5), the relative degree is the number of poles minus the number of zeros , or 6 - 4 = 2.

The full order inverse can lead to a computational drift due to numerical errors in the simulation software. To avoid the computational numerical problem, the reduced order inverse approach is to be used to find the inverse input, as in the work by Boekfah et al., (2016).

To determine the inverse input in the inversion-based method, it is necessary to take the *r*th time derivative so that the input appears, i.e.,

$$\begin{aligned} \frac{d^r y(t)}{dt^r} &= CA^r x(t) + CA^{r-1}Bu(t) \\ &= A_y x(t) + B_y u(t) \end{aligned} \tag{11}$$

The inverse input u_{inv} required to track a sufficiently smooth trajectory y is determined from Eq.(11),i.e.,

$$u_{inv}(t) = B_y^{-1}\left(\frac{d^r y(t)}{dt^r} - A_y x(t)\right) \tag{12}$$

In the reduced order inverse, some components of the state are known when the desired output, $y_d(.)$, and its time derivatives are defined. In particular, the following coordinate transformation can be made.

$$\begin{aligned} z(t) &= \begin{bmatrix} y_d(t) \\ y_d^{(1)}(t) \\ \vdots \\ \frac{d^{(r-1)}}{dt^{(r-1)}} y_d(t) \\ \cdots\cdots \\ \eta(t) \end{bmatrix} = \begin{bmatrix} \zeta_d(t) \\ \cdots \\ \eta(t) \end{bmatrix} = \begin{bmatrix} C \\ CA \\ \vdots \\ CA^{r-1} \\ \cdots\cdots \\ T_\eta(t) \end{bmatrix} x(t) = \begin{bmatrix} T_\zeta \\ \cdots \\ T_\eta \end{bmatrix} x(t) \\ &= Tx(t) \end{aligned} \tag{13}$$

where $\zeta_d(.)$ is the known portion of the state, and η is the unknown portion of the state, and the bottom portion T_η of the coordinate transformation matrix T is chosen such that the matrix T is invertible, leading to the inverse transformation, i.e.,

$$x(t) = T^{-1}\begin{bmatrix} \zeta \\ \cdots \\ \eta \end{bmatrix} = \begin{bmatrix} T_l^{-1} & \vdots & T_r^{-1} \end{bmatrix}\begin{bmatrix} \zeta \\ \cdots \\ \eta \end{bmatrix} = T_l^{-1}\zeta + T_r^{-1}\eta \tag{14}$$

By taking the time derivative of η in Eq.(13) and using the state equation in Eq.(9),the inverse input in Eq.(12) can be rewritten as the output of η in the following inverse system.

$$\dot{\eta}(t) = T_\eta \dot{x}(t) = T_\eta(Ax(t) + Bu(t)) \tag{15}$$

Now the state $x(t)$ in Eq.(14) can be used in Eq.(15) to obtain the inverse system.

$$\dot{\eta}_{inv}(t) = A_{inv}\eta(t) + B_{inv}Y_d(t) \tag{16}$$

$$u_{inv}(t) = C_{inv}\eta(t) + D_{inv}Y_d(t) \tag{17}$$

where η is termed as the internal state, and

$$A_{inv} = T_\eta[A - (BB_y^{-1}A_y)]T_r^{-1}$$

$$B_{inv} = [T_\eta[A - (BB_y^{-1}A_y)]T_l^{-1} \quad \vdots \quad T_\eta BB_y^{-1}]$$

$$C_{inv} = -B_y^{-1}A_y T_r^{-1}$$

$$D_{inv} = [-B^{-1}A_y T_l^{-1} \quad \vdots \quad B_y^{-1}]$$

$$Y_d(t) = \begin{bmatrix} \zeta_d(t) \\ y_d^{(r)}(t) \end{bmatrix}$$

For this particular work of the relative degree r =2, there are therefore four more states to be chosen, and

$\eta(t) = \begin{bmatrix} x_3 \\ x_4 \\ x_5 \\ x_6 \end{bmatrix}$ can be chosen.

where

$$A_y = CA^r = CAA$$

$$B_y = CA^{r-1}B = CAB$$

$$T = \begin{bmatrix} T_\zeta \\ \dots \\ T_\eta \end{bmatrix}$$

$$z(t) = \begin{bmatrix} y_d \\ \dot{y}_d \\ \dots \\ \eta(t) \end{bmatrix} = \begin{bmatrix} \zeta_d(t) \\ \dots \\ \eta(t) \end{bmatrix} = \begin{bmatrix} C \\ CA \\ \dots \\ T_\eta \end{bmatrix} x(t) = \begin{bmatrix} T_\zeta \\ \dots \\ T_\eta \end{bmatrix} x(t)$$

and the matrix T is

$$T = \begin{bmatrix} 11.166 & -0.0511 & 0.8986 & 0.0397 & -0.2050 & 0.0114 \\ 0.2011 & 11.201 & -0.6841 & 0.8852 & -0.3279 & -0.2065 \\ 0 & 0 & 1 & 0 & 0 & 0 \\ 0 & 0 & 0 & 1 & 0 & 0 \\ 0 & 0 & 0 & 0 & 1 & 0 \\ 0 & 0 & 0 & 0 & 0 & 1 \end{bmatrix}$$

The tracking can now be simulated in MATLAB computing software.

5 RESULTS AND DISCUSSIONS

With the initial conditions of being zeros for all the states at time $t = 0$, the tracking results are illustrated in Fig.8 and Fig.9.

5.1 Quantifying Thetracking Errors

To measure the performance of the tracking, the error *E(t)* of tracking, or tracking error can be defined as

$$E(t) = y_a(t) - y_d(t) \tag{18}$$

where $y_a(t)$ is the actual trajectory output and $y_d(t)$ is the desired trajectory output.

Eq.(18) defines an error for each point of time (t) and the error for each point of time is plotted along with the trajectory outputs in Fig. 8 and Fig.9.

Another quantification of tracking performance that can be used to evaluate the tracking is the maximum tracking error $E_{\max}$ and the maximum tracking error is given by

$$E_{\max} = \max|E(t)| \tag{19}$$

To evaluate the overall tracking performance for the entire tracking time of 30 milliseconds, the root mean square error (*RMSE*) can also be used as an index of the tracking performance, and the root mean square error is defined as

$$RMSE = \sqrt{\frac{1}{N}\sum_{i=1}^{N}(y_a(t) - y_d(t))^2} \tag{20}$$

where N is the number of the data points.

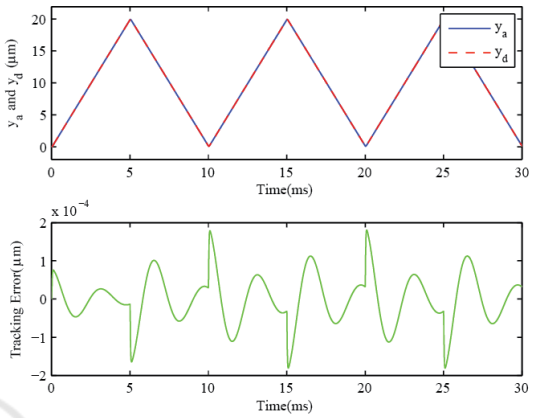

Figure 8: Tracking results for the triangle wave trajectory.

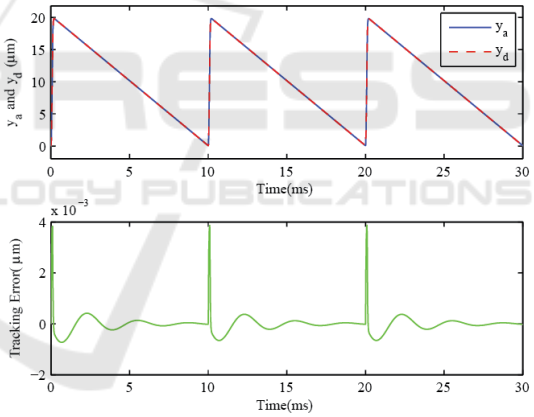

Figure 9: Tracking results for the sawtooth wave trajectory.

5.2 Tracking Performance

From Fig.8 and Fig.9, it can be seen that the tracking error tends to reach a maximum value at the turnarounds of the waves. Table 2 shows very small values of the $E_{\max}$ and the *RMSE* values of tracking the triangle wave and the saw tooth wave and indicates very good tracking performances. In particular, $E_{\max}$ values are very small, compared to the wave amplitude of 10 μm i.e., 1.81×10^{-4} μm for the triangle wave and 3.87×10^{-3} μm for the sawtooth wave. This reports that the tracking

performance is very good. Table 2 also indicates that tracking the saw tooth wave (with sharper turnarounds at the corner, compared to the triangle wave) yields larger values of the $E_{\max}$ and the *RMSE* values, compared to tracking the triangle wave. In other words, tracking of the sawtooth wave is more difficult than that of the triangle wave.

Table 2: Maximum Error ($E_{\max}$) and Root Mean Square Error (*RMSE*).

Wave Type	$E_{\max}$ (μm)	*RMSE* (μm)
Triangle	1.81×10^{-4}	6.50×10^{-5}
Sawtooth	3.87×10^{-3}	4.11×10^{-4}

6 ROBUSTNESS OF TRACKING

To delve into the robustness against unmodeled dynamics, modeling error, or disturbance, for this particular study, it is assumed that the natural frequency ω_n and the damping ratio ζ are increased by some percentage.

There are four cases that are investigated for each trajectory for the study of robustness.

Case [1]: ω_n and ζ are not changed and their numerical values are shown in Table 1.The study of this case was completed in Section 5.

The plots were shown in Fig.8 for the triangle case and in Fig.9 for the sawtooth case. The tracking errors were quantified and shown in Table 2. This is a reference case for the other three cases.

Case [2]: ω_n and ζ are increased by 3.2 %.

The plots are shown in Fig. 10 for the triangle case and in Fig.13 for the sawtooth case.

Case [3]: ω_n and ζ are increased by 5.0 %.

The plots are shown in Fig.11 for the triangle case and in Fig.14 for the sawtooth case.

Case [4]: ω_n and ζ are increased by 10.0 %.

The plots are shown in Fig.12 for the triangle case and in Fig.15 for the sawtooth case.

For all cases, the tracking errors are quantified and shown in Table 3 for the case of the triangle trajectory and Table 4 for the case of the sawtooth trajectory.

From Fig.10 to Fig.15, Table 3 and Table 4, it is observed that

1. $E_{\max}$ is still less than 10% of the peak to peak amplitude of 20 micron if the increases in the natural frequency and the damping ratio are less than 5% for the triangle trajectory, and $E_{\max}$ is still less than 10% of the peak to peak amplitude of 20 micron if the increases in the natural frequency and the damping ratio are less than 3.2 % for the sawtooth trajectory.
2. $E_{\max}$ and *RMSE* increase as the percentage of change in the natural frequency and the damping ratio is increased.
3. The tracking is quite sensitive to the change in the natural frequency and the damping ratio. Particularly, if the increases by 10%, the tracking gets worse.
4. The maximum error tends to occur at the sharp corner of the trajectories.
5. The actual trajectory of the sawtooth oscillates obviously if there are changes in the natural frequency and the damping ratio.

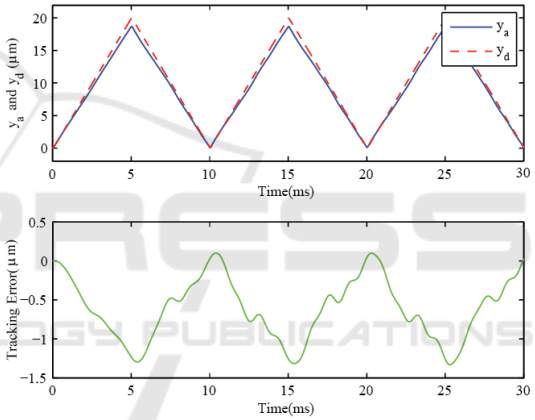

Figure 10: Tracking results for the triangle wave trajectory in case [2].

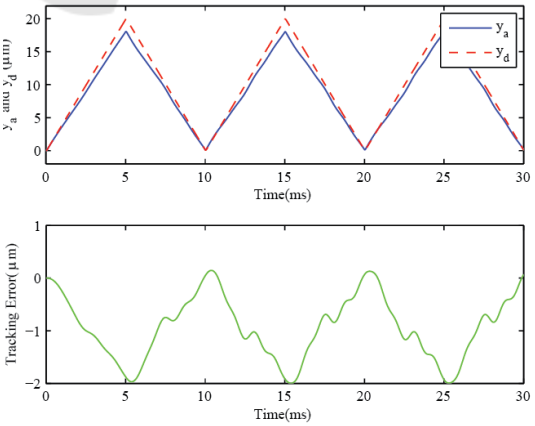

Figure 11: Tracking results for the triangle wave trajectory in case [3].

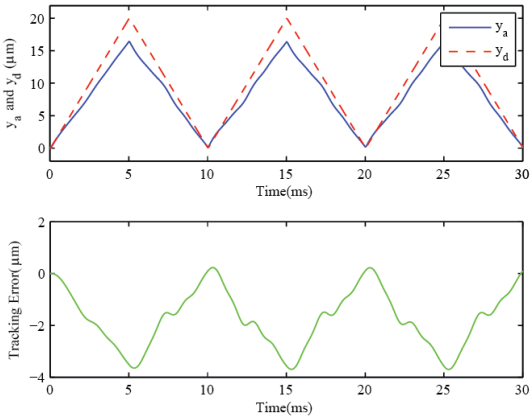

Figure 12: Tracking results for the triangle wave trajectory in case [4].

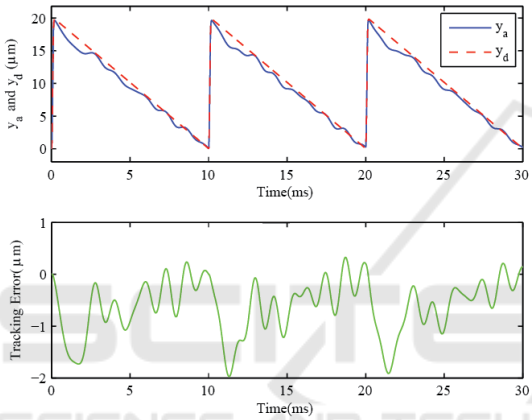

Figure 13: Tracking results for the sawtooth wave trajectory in case [2].

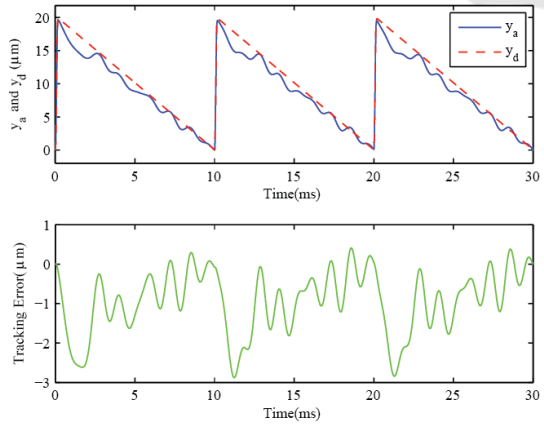

Figure 14: Tracking results for the sawtooth wave trajectory in case [3].

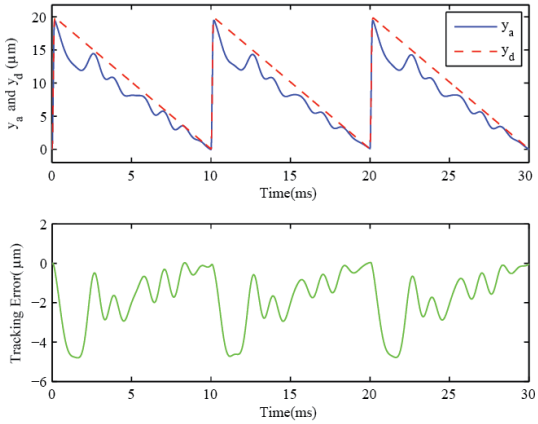

Figure 15: Tracking results for the sawtooth wave trajectory in case [4].

Table 3: Maximum Error ($E_{\max}$) and Root Mean Square Error (*RMSE*) for triangle trajectory.

Case	$E_{\max}$ (μm)	*RMSE* (μm)
[1]	1.81×10^{-4}	6.50×10^{-5}
[2]	1.331	7.30×10^{-1}
[3]	1.99	1.11
[4]	3.70	2.06

Table 4: Maximum Error ($E_{\max}$) and Root Mean Square Error (*RMSE*) for sawtooth trajectory.

Case	$E_{\max}$ (μm)	*RMSE* (μm)
[1]	3.87×10^{-3}	4.11×10^{-4}
[2]	1.97	8.03×10^{-1}
[3]	2.88	1.22
[4]	4.80	2.21

7 CONCLUSIONS

This article presents an inversion-based control approach to tracking wave trajectories. The interesting challenge is that the tracking involves the trajectories that possess a high frequency, a microscale amplitude, sharp turnarounds at the corners. The model or transfer function of a piezoactuator is obtained experimentally from the frequency response by using a dynamic signal analyzer. Under the inversion-based control scheme and the model obtained ,the tracking is simulated in MATLAB. The main contributions of this work are to show that (1) the model and the controller achieve a good tracking performance measured by the root

mean square error (*RMSE*) and the maximum error (E_{max}), (2) the maximum error tends to occur at the sharp corner of the trajectories, (3) tracking the sawtooth wave yields larger *RMSE* and E_{max} values, compared to tracking the triangle wave, and (4) in terms of robustness against modeling error or unmodeled dynamics, E_{max} is still less than 10% of the peak to peak amplitude of 20 micron if the increases in the natural frequency and the damping ratio are less than 5% for the triangle trajectory and E_{max} is still less than 10% of the peak to peak amplitude of 20 micron if the increases in the natural frequency and the damping ratio are less than 3.2 % for the sawtooth trajectory.

There is still room for developing the tracking and improving the tracking performance, in particular for the robustness against unmodeled dynamics or disturbances by means of adding a feedback control to the inversion-based control.

ACKNOWLEDGEMENTS

The author of the article would like to sincerely thank Assumption University of Thailand for supporting the research.

REFERENCES

Beschi, M., Dormido, S., Sanchez, J., Visioli, A., and Yebra, L. J.,(2014) 'Event-Based PI plus Feedforward Control Strategies for a Distributed Solar Collector field', *IEEE Transactions on Control Systems Technology*, Vol. 23, No. 4, July 2014,pp. 1615–1622.

Boekfah, A., and Devasia, S.,(2016) 'Output-Boundary Regulation Using Event-Based Feedforward for Nonminimum-Phase Systems', *IEEE Transactions on Control Systems Technology*, Vol.24,No.1, January 2016, pp265-275.

Devasia, S., (2002). 'Should Model-Based Inverse Inputs Be Used as Feedforward Under Plant Uncertainty?', *IEEE Transactions on Automatic Control*, Vol.47, No.11, November 2002,pp1865-1871.

Dunne, F., Pao, L. Y., Wright, A. D., Jonkman, B., and Kelley, N.,(2011) 'Adding Feedforward Blade Pitch Control to Standard Feedback Controllers for Load Mitigation in Wind Turbines', *Mechatronics*, Vol. 21, No. 4, June 2011, pp. 682–690.

Hirschorn, R. M., (1979). 'Invertibility of Multivariable Nonlinear Control Systems', *IEEE Transactions on Automatic Control*, Vol.AC-24, No.6, December 1979,pp855-865.

Kongthon, J., Chung, J.-H., Riley, J., and Devasia, S.,(2011)'Dynamics of Cilia-Based Microfluidic Devices', *ASME Journal of Dynamic Systems, Measurement and Control*,Vol. 133, September 2011,pp.051012-1-051012-11.

Kongthon, J., and Devasia, S., (2013) 'Iterative Control of Piezoactuator for Evaluating Biomimetic, Cilia Based Micromixing', *IEEE/ASME Transactions on Mechatronics*, Vol.18, No. 3, June 2013, pp 944-953.

Kongthon, J., McKay, B.,Iamratanakul, D., Oh, K., Chung, J.-H., Riley, J., and Devasia, S.,(2010) 'Added-Mass Effect in Modeling of Cilia-Based Devices for Microfluidic Systems', *ASME Journal of Vibration and Acoustics*, Vol.132, No.2, April 2010, pp.024501–1–024501–7.

Martin, P., Devasia, S., and Paden, B., (1996). 'A Different Look at Output Tracking: Control of a VTOL Aircraft', *Automatica*, Vol. 32, No. 1,pp. 01-107.

Meckl, P. H.,and Kinceler, R.,(1994) 'Robust Motion Control of Flexible Systems Using Feedforward Forcing Functions', *IEEE Transactions on Control Systems Technology*, Vol. 2, No. 3, September 1994,pp. 245–254.

Moallem, M., Kermani, M. R., Patel, R. V., and Ostojic, M.,(2004) 'Flexure Control of a Positioning System Using Piezoelectric Transducers', *IEEE Transactions on Control Systems Technology.*, Vol. 12, No. 5,September 2004,pp. 757–762.

Peng, H., and Tomizuka, M., (1993) 'Preview Control for Vehicle Lateral Guidance in Highway Automation', *ASME Journal of Dynamic Systems, Measurement and Control*, Vol. 115, No. 4, December 1993, pp.679–686.

Piazzi, A., and Visioli, A.,(2001) 'Optimal Inversion-Based Control for the Setpoint Regulation of Nonminimum-Phase Uncertain Scalar Systems', *IEEE Transactions on Automatic Control*,Vol. 46, October 2001, No. 10, pp. 1654–1659.

Silverman, L. M.,(1969) 'Inversion of Multivariable Linear Systems', *IEEE Transactions on Automatic Control*, Vol.AC-14,No.3,June 1969,pp270-276.

Yang, X., Garratt, M., and Pota, H., (2011) 'Flight Validation of a Feedforward Gust-Attenuation Controller for an Autonomous Helicopter', *Robotics and Autonomous Systems*, Vol. 59, No. 12, December 2011, pp. 1070–1079.